RICHARD F. GASPAROVIC, DONALD R. THOMPSON, and JOHN R. APEL

SYNTHETIC APERTURE RADAR IMAGING OF SHIP-GENERATED INTERNAL WAVES

An experiment to investigate synthetic aperture radar imaging of ship-generated internal waves was conducted in Loch Linnhe, Scotland, in September 1987. Data acquired are being used to test models of internal wave generation and radar imaging.

INTRODUCTION

Just before the turn of the century, the great Norwegian meteorologist Vilhelm W. Bjerknes advanced a tentative explanation for an interesting hydrodynamic phenomenon often observed when a slow-moving ship traverses a body of water that has a large density change just below the surface.[1] The phenomenon, known as the "dead water" effect, is commonly encountered where a shallow layer of fresh water overlays salt water and manifests itself as greatly increased drag on the ship, requiring an increase in propulsive power to maintain speed. Bjerknes suggested that when a ship moves through density-stratified water, the displacement of water by the hull can excite subsurface waves, known as internal waves, by a process analogous to the hull-generation of surface waves at the air/water interface. The work done in generating these waves either causes the vessel to lose speed or requires increased propulsive power to maintain speed. In extreme situations, the forward motion of the vessel is retarded significantly, hence the origin of the term "dead water." His student, V. W. Ekman, subsequently demonstrated in a classic piece of experimental and theoretical research, that internal waves could indeed exist and could account for the drag.

The internal waves generated by the ship are organized into a distinct pattern along its track, in the same way that the ship-generated surface waves appear in the well-known Kelvin wave pattern. In this issue, Dysthe and Trulsen discuss details of the internal wave pattern, which manifests itself by the alterations of small ripples on the surface via a hydrodynamic interaction between near-surface currents induced by the internal waves and the ambient surface wave field. Striking examples of these patterns can be seen in the photographs published by Hughes and Grant.[2] Similar patterns appear in radar images because the surface ripples strongly influence the backscattering of microwave energy from a water surface. By combining oceanographic measurements with hydrodynamic models for the internal wave generation and wave–current interaction processes and electromagnetic models for radar scattering, it is possible to analyze these images and to test theories for radar imaging of a variety of ocean phenomena. Such testing was the objective of a joint United States–United Kingdom experiment conducted in Loch Linnhe, Scotland, in September 1987.

EXPERIMENT DESCRIPTION

Loch Linnhe, located in northwestern Scotland, is a large loch that begins in the Scottish Highlands and flows southwest to the Atlantic Ocean. In summer, the upper part of the loch has a shallow layer of fresh river and runoff water a few meters deep overlying salty seawater, which extends to the bottom. The UK experiment team from the Royal Aerospace Establishment (RAE) at Farnborough selected this loch as the experiment site because of its environment and the loch's access to the sea, which allowed a Royal Marine Auxiliary Service oceangoing tug, RMAS *Roysterer*, to serve as the vessel to generate internal waves.

Test operations were based at the Underwater Centre in Fort William, a small town at the loch's upper end. An instrumentation site was established about 8 km down the loch, where research vessels, pontoons, and a buoy were deployed for *in situ* oceanographic and meteorological measurements. A CV-580 aircraft with a C-band (5.31-GHz) synthetic aperture radar (SAR) operated by the Canada Centre for Remote Sensing was used to image the internal wave pattern from the *Roysterer*. The radar had a digital data acquisition system to record the raw radar return for subsequent ground processing. An RAE helicopter was also used to photograph the pattern.

The experiment extended over 10 days of test operations between 2 and 22 September 1987. A typical data collection sequence consisted of the *Roysterer* running up and down the loch past the instrumentation site while the aircraft overflew the area to record radar imagery and to photograph the internal wave pattern. Test operations were directed by RAE personnel. Participants from the United States included scientific teams from APL and TRW. Members of the Scottish Marine Biological Association (SMBA) at Oban also participated.

The APL investigators provided a large instrumented spar buoy equipped with conductivity–temperature–depth (CTD) sensors and current meters to measure the internal-wave characteristics; it also had meteorological and wave sensors to measure surface data. Other CTD

measurements were made with RAE sensor strings suspended from three pontoons and with sensors on the SMBA research vessel *Calanus*. The TRW team supplied a scanning laser wave-slope sensor that was operated from a second research vessel, *Loch Nevis*. The sensor measured the changes in the surface wave ripples induced by the internal waves. Besides participating in the experiment, APL personnel were responsible for processing the SAR data into digital imagery for analysis by members of the U.S. experiment team.

INTERNAL WAVE MEASUREMENTS

Depth profiles of conductivity and temperature were taken daily to compute the ambient water column density, $\rho(z)$, as a function of depth, z, and the Brunt-Väisälä (B-V) frequency

$$N(z) = \sqrt{\frac{-g}{\rho(z)} \frac{d\rho(z)}{dz}} , \quad (1)$$

where g is the gravitational acceleration, and z is positive upward. The B-V frequency characterizes the density structure of the ambient water column and, in particular, determines the properties of the ship-generated internal waves. Figure 1 shows typical profiles of the density anomaly, $\sigma_t(z)$, where $\sigma_t(z) = \rho(z) - \rho_0$ and ρ_0 is the density of fresh water, and of the B-V frequency, $N(z)$. Note that the maximum B-V frequency occurs at a depth of about 3 m and has a value of about 80 cycles/h. It is precisely this shallow density gradient that allowed the *Roysterer*, with a 6-m draft, to be an efficient internal wave generator in Loch Linnhe.

The *in situ* measurements showed that the vertical motion induced within the water column by internal waves was predominantly in the same direction at all depths; that is, the internal waves were mostly mode 1 waves, with the maximum displacement occurring near the depth of the maximum B-V frequency. For these conditions, the isopycnal (constant-density) vertical displacement, $\eta(x,z,t)$, induced by a group of internal waves can be written as

$$\eta(x,z,t) = \sum_c W_c^{(1)}(z)\, \xi_c^{(1)}(x,t) , \quad (2)$$

where x is a horizontal coordinate and the subscript c refers to the phase speed of an individual wave in the group. The mode 1 eigenfunction, $W_c^{(1)}(z)$, is a particular solution of the eigenvalue equation,

$$c^2 \frac{d^2}{dz^2} W_c^{(1)}(z) + N^2(z)\, W_c^{(1)}(z) = \omega^2 W_c^{(1)}(z) , \quad (3)$$

subject to the boundary conditions $W_c^{(1)}(0) = W_c^{(1)}(-D) = 0$, where the surface is at $z = 0$ and the bottom is at $z = -D$. The functions $\xi_c^{(1)}(x,t)$ in Equation 2 can be estimated by solving Equation 2 using the measured isopycnal displacements at each sensor depth, z_s, and the value of $W_c^{(1)}(z_s)$ computed from Equation 3 for the appropriate wave phase speed, c, and frequency, ω. Figure 2 shows the eigenfunction, $W_c^{(1)}(z)$, for a typical internal wave phase speed of 0.4 m/s.

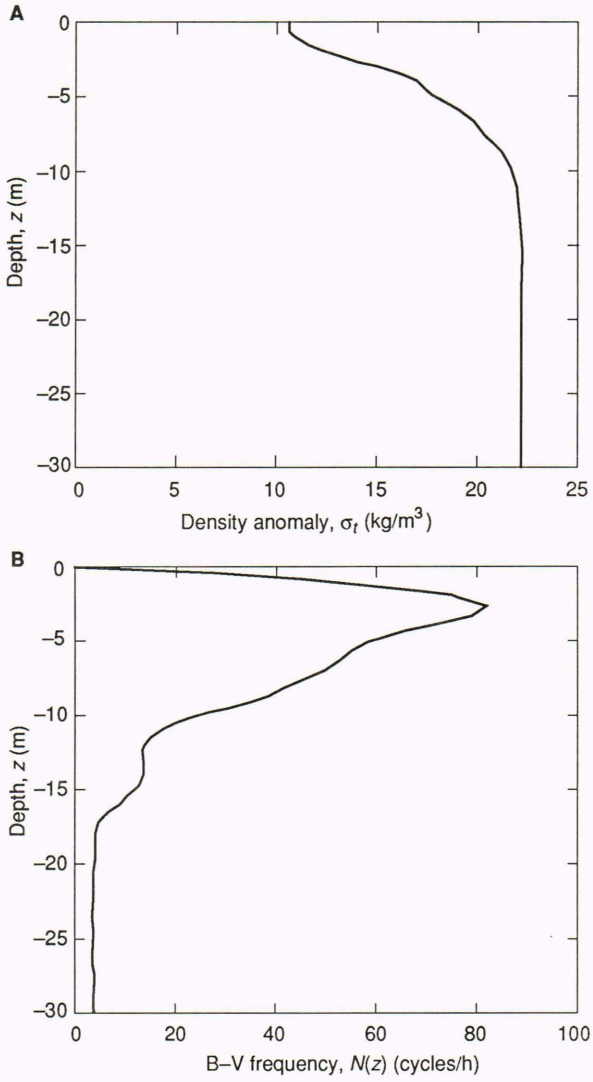

Figure 1. Depth profiles of density anomaly (A) and Brunt-Väisälä frequency (B).

The colored curve in Figure 3 shows an isopycnal displacement inferred from the CTD time series at a depth of 5.3 m when part of the internal wave pattern propagated past the APL spar buoy. Three prominent internal wave oscillations can be seen, with amplitudes between 0.3 and 0.6 m. The black curve in Figure 3 is an analytical representation of the measured displacement that is used to compute the surface current induced by this wave group. The procedure for computing the surface current is straightforward; it uses the equation of continuity for incompressible flow to compute the current field gradients, which are then integrated to yield the horizontal current and current gradient (or strain rate) at the surface (Fig. 4). Here, the time dependence

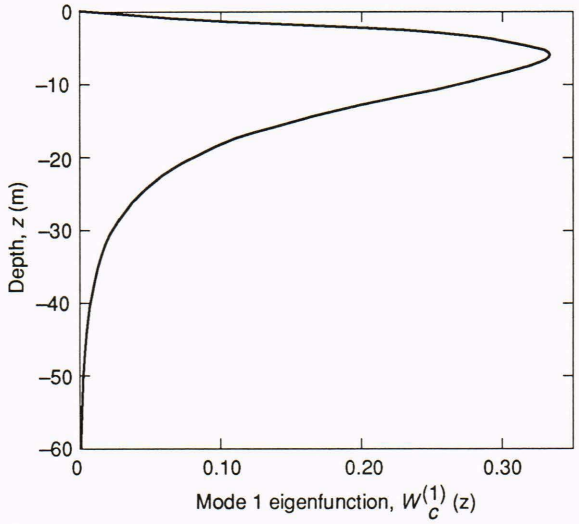

Figure 2. Internal-wave eigenfunction for a wave speed of 0.4 m/s.

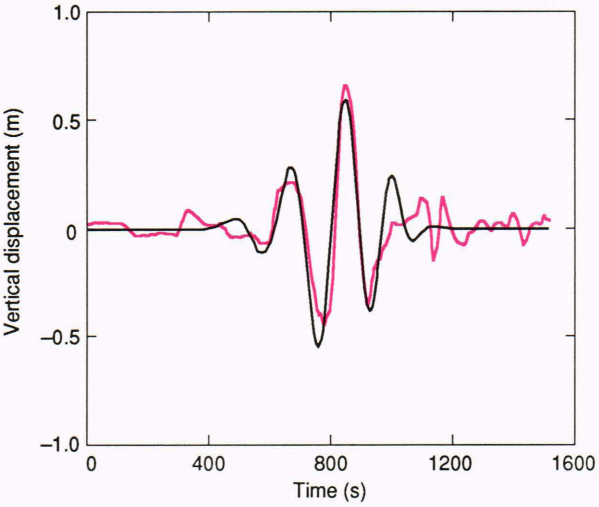

Figure 3. Isopycnal vertical displacement at a depth of 5.3 m for a ship-generated internal wave group. The colored curve is inferred from the data; the black curve is an analytical representation of the data.

of the isopycnal displacements measured at a fixed location has been transformed to the spatial pattern of the surface current using the internal-wave propagation speed. Note that the maximum currents range from about 0.015 to 0.030 m/s, with peak strain rates of approximately 0.002 s^{-1}, which are typical values for the internal waves generated by the *Roysterer* during the experiment. These currents modulate the ambient surface wave spectrum, thereby rendering the internal wave pattern visible to the radar.

SURFACE WAVE MODULATIONS

To estimate the effect of the internal wave pattern on the radar return, it is necessary first to compute the modifications to the surface wave spectrum. Previous

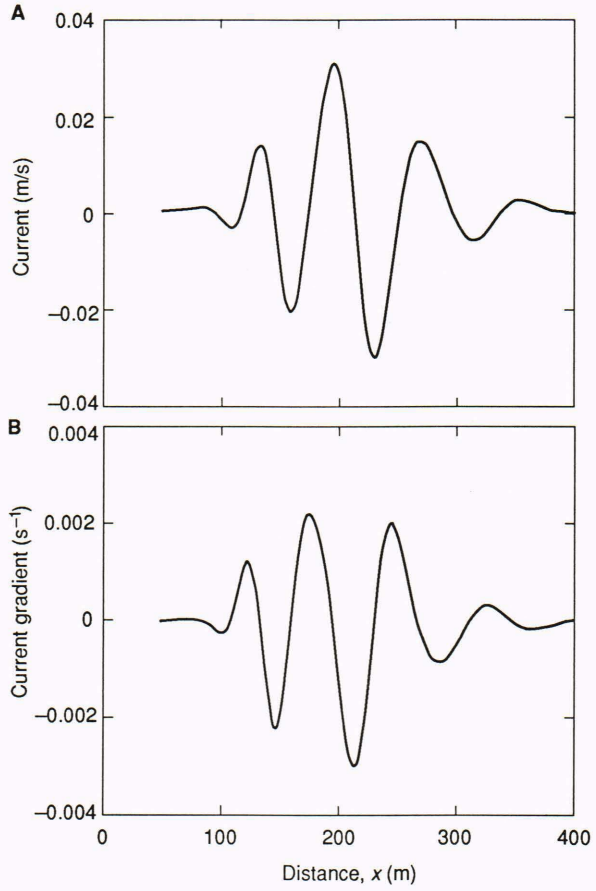

Figure 4. Surface current (A) and current gradient or strain rate (B) pattern for the isopycnal displacements in Figure 3.

experiments have demonstrated that the surface wave modulations can be obtained by solving an action-balance equation of the form

$$\frac{d}{dt}N(\mathbf{k};\mathbf{x},t) = \beta(\mathbf{k})\, N(\mathbf{k};\mathbf{x},t)\left[1 - \frac{N(\mathbf{k};\mathbf{x},t)}{N_0(\mathbf{k})}\right], \quad (4)$$

where $N(\mathbf{k};\mathbf{x},t)$ is the spectral density of the surface wave action for wave number $\mathbf{k}$ at horizontal position $\mathbf{x}$ and time t, $\beta(\mathbf{k})$ is the surface-wave relaxation rate, and $N_0(\mathbf{k})$ is the equilibrium (no-current) ambient action spectrum.[3,4] The time dependencies of $\mathbf{x}$ and $\mathbf{k}$ are given by

$$\frac{dx_i}{dt} = \frac{\partial \omega_0}{\partial k_i} + U_i \quad (5a)$$

$$\frac{dk_i}{dt} = -k_j \frac{\partial U_j}{\partial x_i}, \quad (5b)$$

where the indices i and j run from 1 to 2 and repeated indices are summed. The quantity $\mathbf{U}(\mathbf{x},t)$ represents the surface current field induced by the internal waves. The action spectrum is related to the surface wave height spectrum, $S(\mathbf{k};\mathbf{x},t)$, by

$$N(\mathbf{k};\mathbf{x},t) = \frac{\rho_s \omega_0}{|\mathbf{k}|} S(\mathbf{k};\mathbf{x},t) , \quad (6)$$

where ρ_s is the surface density and ω_0 is the wave frequency in a local rest frame corresponding to wave number $\mathbf{k}$.

The surface wave modulations induced by internal waves can extend over a broad range of wavelengths, depending on the magnitude and spatial extent of the current pattern and on the wind speed. Centimeter-scale and shorter waves generally undergo very small modulations because they are tightly coupled to the wind, which tends to force them quickly back into equilibrium. Very long surface waves move rapidly through localized current patterns, and their modulations are limited by the available interaction time. The waves most affected by internal waves are those with an interaction time comparable to the relaxation time, $\beta^{-1}(\mathbf{k})$, a function that depends also on the wind speed. For the types of internal waves generated in the Loch Linnhe experiment, surface waves with wavelengths from about 0.05 to 5 m experience the largest modulations.

To solve Equation 4, a model equilibrium wave spectrum is chosen that is appropriate for the measured wind conditions, along with an expression for $\beta(\mathbf{k})$ from Hughes.[3] Figure 5 shows the computed modulation (defined as the ratio of the spectral density in the presence of the current to its ambient value) of surface waves with wavelengths of 0.06 m (Fig. 5B) and 0.90 m (Fig. 5C), caused by the current shown in Figure 5A. A wavelength of 0.06 m corresponds to the Bragg wavelength, $\lambda_B = \lambda_{RF}/(2 \sin \theta)$, for the C-band radar ($\lambda_{RF} = 5.65$ cm) at an incidence angle, θ, of 29°. A modulation of greater than unity indicates an increase in the amplitude of the particular wave component, or enhanced surface-wave roughness. Similarly, smooth areas on the surface are associated with modulations of less than unity where the wave amplitude has decreased. Note that the 0.9-m wave has a substantial modulation, indicating that the long-wave tilting of the short waves that scatter the radar energy must be taken into account when calculating the radar backscatter modulations.[5]

RADAR IMAGERY

It follows from the foregoing discussion that the pattern of internal waves generated by the ship will induce alternating regions of enhanced and diminished wave activity on the water surface. When the pattern is illuminated with microwave energy, the backscattered signal will increase or decrease depending on the changes in wave activity, thereby mapping out the pattern as intensity variations in a radar image. Figure 6 shows a radar image obtained with the C-band SAR and recorded on 17 September when the aircraft flew parallel to the ship track while the ship was traveling from left to right at 1.0 m/s. The internal waves appear as a V-shaped pattern behind the *Roysterer,* which is the large bright target near the right edge of the image. The other bright targets in the upper half of the pattern are the research vessels, pontoons, and buoy deployed at the instrumentation site.

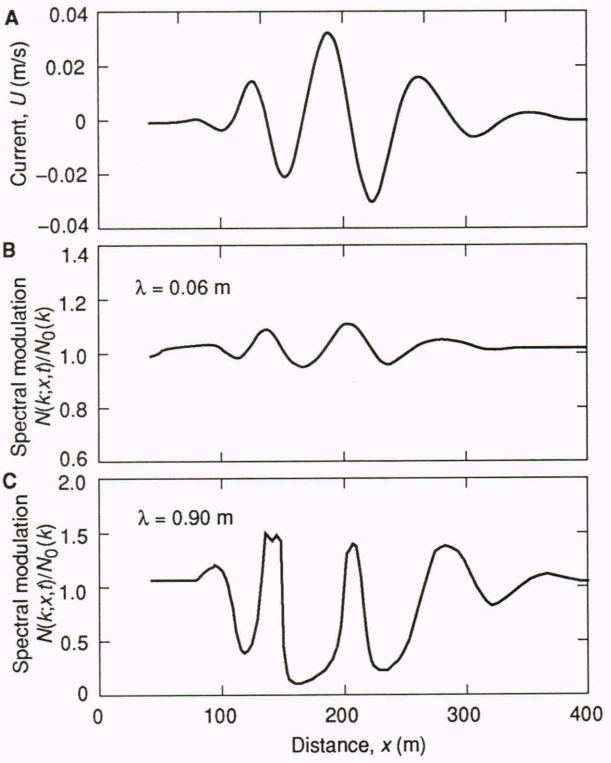

Figure 5. Spectral modulations of 0.06-m (B) and 0.90-m (C) surface waves by the surface current pattern (A). The wavelength of 0.06 m corresponds to the Bragg wavelength.

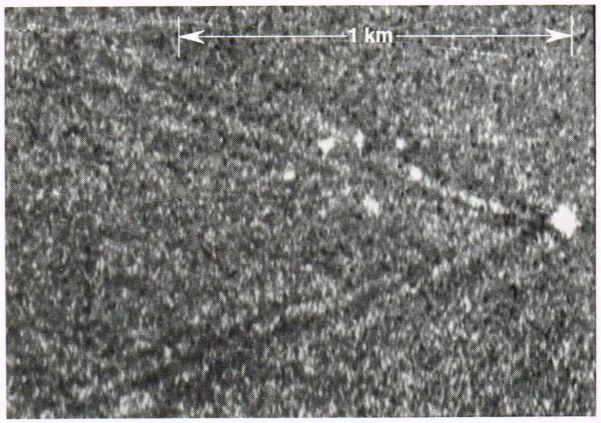

Figure 6. C-band synthetic aperture radar image of an internal wave pattern from a ship moving at a speed of 1 m/s. The image is in ground range coordinates and has the scale shown.

The propagation speed of each wave in the pattern determines the angle between the wave and the ship's track. Because the pattern is stationary in a coordinate system moving with the ship, it follows that the half-angle, ϕ, of the pattern is given approximately by

$$\sin \phi = \frac{c}{v_s} , \quad (7)$$

where c is the phase speed of the outermost wave and v_s is the ship speed. The half-angle of the outermost

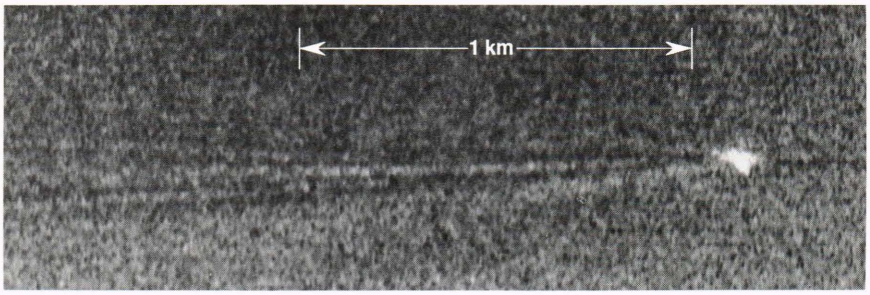

Figure 7. C-band synthetic aperture radar image of internal waves from a ship moving at 6 m/s.

wave in the pattern in Figure 6 was measured in the SAR image as about 27°, implying a phase speed of 0.45 m/s, in good agreement with the value of 0.42 m/s estimated from the *in situ* measurements. Note that, according to Equation 6, if the wave speed remains constant, the included angle of the pattern will decrease as the ship speed increases. This speed dependence of the pattern can be seen by comparing Figure 7 (recorded on 16 September when the ship speed was 6 m/s) with Figure 6.

An important question being addressed in the analysis of the Loch Linnhe data is whether the observed C-band SAR image intensity modulations can be predicted by using the same hydrodynamic and electromagnetic models previously applied to L-band (1.25-GHz) and X-band (9.35-GHz) imagery of internal waves.[6,7] The hydrodynamic model for the surface wave modulation is summarized in the preceding section. These wave modulations are used as inputs to a two-scale composite scattering model to calculate the backscattered electromagnetic field.[5] The model includes contributions from both the small-scale waves (the so-called Bragg waves) and the longer surface waves, which tilt the small waves.

Figure 8 compares the observed and calculated image-intensity modulations for a segment of the internal wave pattern shown in Figure 6. The selected image segment is located immediately to the left of the bright targets at the instrumentation site, extending about 180 m along the wave pattern. The black curve in Figure 8 represents the image intensity averaged along the wave fronts in this segment of the pattern. Modulations greater than unity appear as bright features in the SAR image; dark features have modulations of less than unity. The colored curve is the predicted modulation from the model calculations. The agreement is considered acceptable and is comparable to that found for other radar frequencies in other internal wave imaging experiments.[6,8] Similar agreement between observed and predicted SAR modulations has been found for images recorded during other data sessions in the Loch Linnhe experiment.

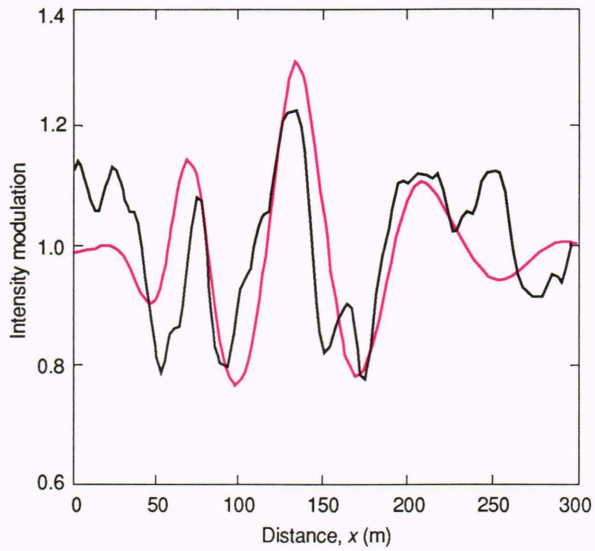

Figure 8. Plot of the intensity modulations of a synthetic aperture radar image for an image segment of Figure 6, extending about 180 m along wave fronts to the left of the instrumentation site. The black curve represents the SAR image intensity averaged along the wave fronts; the colored curve represents the modulations calculated from the model.

CONCLUSION

The Loch Linnhe experiment produced many radar images of the patterns of internal waves generated by ships and provided the first opportunity to obtain digital C-band SAR imagery of internal wave signatures for quantitative testing of radar-imaging models. The results obtained have shown that the pattern geometry is consistent with pre-test predictions, although the observed amplitudes of the internal waves have yet to be explained. The magnitudes of the radar signatures in several images from different data sessions are in good agreement with predictions from models used to interpret internal wave signatures at other radar frequencies. Additional analyses of these data and data from a second experiment conducted in August 1989 are in progress. The results are expected to yield valuable contributions to our understanding of the complex process by which oceanographic phenomena are manifested in radar imagery.

REFERENCES

[1] Ekman, V. W., "On Dead Water," Chap XV, Vol. V, *The Norwegian North Polar Expedition, 1893-96, Scientific Results*, F. Nansen, ed., Longmans, Green, and Co., London, New York, Bombay (1906).

[2] Hughes, B. A., and Grant, H. L., "The Effect of Internal Waves on Surface Wind Waves, 1, Experimental Measurements," *J. Geophys. Res.* **83**, 443-454 (1978).

[3] Hughes, B. A., "The Effects of Internal Waves on Surface Wind Waves, 2, Theoretical Analysis," *J. Geophys. Res.* **83**, 455-465 (1978).

[4] Thompson, D. R., Gotwols, B. L., and Sterner, R. E., II, "A Comparison of Measured Surface Wave Spectral Modulations with Predictions from a Wave-Current Interaction Model," *J. Geophys. Res.* **93**, 12,339-12,343 (1988).

[5]Thompson, D. R., "Calculation of Radar Backscatter Modulations from Internal Waves," *J. Geophys. Res.* **93**, 12,371–12,380 (1988).
[6]Gasparovic, R. F., Apel, J. R., and Kasischke, E. S., "An Overview of the SAR Internal Wave Experiment," *J. Geophys. Res.* **93**, 12,304–12,316 (1988).
[7]Holliday, D., St-Cyr, G., and Woods, N. E., "Comparison of a New Radar Ocean Imaging Model with SARSEX Internal Wave Image Data," *Int. J. Remote Sensing* **8**, 1423–1430 (1987).
[8]Hughes, B. A., and Dawson, T. W., "Joint Canada–U.S. Ocean Wave Investigation Project: An Overview of the Georgia Strait Experiment," *J. Geophys. Res.* **93**, 12,219–12,234 (1988).

ACKNOWLEDGMENTS—Numerous individuals contributed to the success of the Loch Linnhe experiment. Brian Barber and Jonathon Perry were the principal Royal Aerospace Establishment investigators responsible for overall direction of the experiment. Anton Edwards of the Scottish Marine Biological Association coordinated operations on the *Calanus* and supplied CTD profiles. Carl Nelson, David Mosher, Christian Keller, and Marcos Gonzalez provided APL instrumentation and data acquisition support. Dale Griffith and Christopher Vogt of APL processed the SAR data from the Canada Centre for Remote Sensing. The author acknowledges the support of Ronald Repka and Richard Whiting of the Defense Advanced Research Projects Agency.

THE AUTHORS

RICHARD F. GASPAROVIC's biography can be found on p. 294.

DONALD R. THOMPSON's biography can be found on p. 338.

JOHN R. APEL's biography can be found on p. 294.